ICARUS **134,** 279–291 (1998)
ARTICLE NO. IS985958

Shadows on a Planetary Surface and Implications for Photometric Roughness

Michael K. Shepard

Department of Geography and Earth Science, 400 East Second Street, Bloomsburg University, Bloomsburg, Pennsylvania 17815
E-mail: mshepard@planetx.bloomu.edu

and

Bruce A. Campbell

Center for Earth and Planetary Studies, MRC 315, National Air and Space Museum, Smithsonian Institution, Washington, DC 20560

Received August 25, 1997; revised February 9, 1998

We advocate the use of fractal surface statistics as a simple, quantitative, and general model for planetary surface roughness. We determine the shadowing behavior of a wide range of fractal surfaces using computer simulations, and present an empirical function that reproduces their observed behavior within statistical uncertainties. We compare the shadowing behavior of fractal surfaces to four analytic shadowing models for random surfaces and find that three of these, including the Hapke (1984, *Icarus* 59, 41–59) model, are well approximated by specific cases of a general fractal surface model. In addition, we demonstrate that a fractal surface model provides a way of quantitatively verifying and extending previous interpretations of the Hapke (1984) roughness parameter. We hypothesize that the scale which dominates surface shadowing, and by extension photometric roughness, is the smallest surface scale for which shadows exist and that this scale is a function of intrinsic physical parameters such as the single scattering albedo and particle phase function. If correct, a major implication of this hypothesis is that photometric roughness may have different physical meanings on different surfaces.

Key Words: **photometry; surfaces; planets; computer techniques.**

I. INTRODUCTION AND RATIONALE

An important goal of planetary remote sensing is to quantitatively "link" scattering parameters extracted from remote observations to physical parameters that can be measured *in situ*. This link requires the utilization of at least two types of models: (1) a model that describes the interaction between electromagnetic radiation and idealized surfaces, often chemically homogeneous and smooth at wavelength scales; and (2) a model that describes specific variations in the idealized behavior of the surface, e.g., chemical inhomogeneities and/or surface roughness. In planetary applications, these models are combined into a general surface scattering model; common examples include the Hagfors quasi-specular model for radar (Hagfors 1964) and the Hapke (1981, 1984) model for photometry. In order for geologic inferences based on a general scattering model to be sound, each model component must be realistic, i.e., based upon physical principles and/or empirically observed behavior, and general enough to encompass the widest range of surface types one is likely to encounter. Although the interactions between electromagnetic waves and idealized surfaces have been reasonably well characterized for over a century, we suggest that significant improvements can still be made in the characterization of geologic surface roughness. In this paper, we advocate the use of fractals as a simple, quantitative, and general model for surface roughness. The major advantage of fractals over all surface models currently in use is that they explicitly account for changes in surface roughness with scale.

Our purpose in this paper is to:

(1) demonstrate that fractals are capable of quantifying observed surface roughness;

(2) generate a shadowing function for fractal surfaces—a first step in the use of fractal surfaces for general scattering models;

(3) demonstrate that fractal surfaces are more general descriptors of surface roughness than models currently employed by comparing their shadowing behaviors;

(4) examine the interpretation of scale in generalized scattering models that utilize shadowing functions, most notably the Hapke (1984) photometric model; and

(5) present a new hypothesis for the physical interpretation of photometric roughness. Although our ultimate goal

0019-1035/98 $25.00

is to analytically incorporate fractal surface behavior into general scattering models, that is not a goal of this paper. Rather, we wish to demonstrate that the level of work necessary to incorporate fractal behavior into these models is justified by potential benefits and take some initial steps toward its realization.

In what follows, we briefly describe fractal surfaces and illustrate their utility in representing natural surfaces. Following that, we begin the process of integrating a fractal surface model into a general scattering model by numerically determining the shadowing function for fractal surfaces observed at nadir. To demonstrate that a fractal surface model is more general in scope than surface models previously utilized, we compare its shadowing behavior to that of four published surface roughness models, including the well known Hapke (1984) model. Finally, we address the question of scale in the Hapke (1981, 1984, 1986) photometric model using the results of the shadowing computation, illustrate how a fractal model may quantitatively verify previous interpretations of the physical meaning of the Hapke roughness parameter, and conclude with some further speculations on this topic.

II. FRACTAL SURFACE ROUGHNESS MODELS

A wide variety of surface models have been or are currently utilized in planetary remote sensing. In the broadest possible terms, these can be broken into three major categories. Models in the first category we call ''deterministic'' since they are composed of one or more well defined elements in a predetermined arrangement. Periodic surfaces, e.g., sinusoidal, sawtooth, or rectangular corrugated surfaces (cf. Beckmann and Spizzichinno 1963), are common forms of this surface type. In the second category, the surface is also composed of well-defined elements, but there may be random quantities of elements, they may have random sizes and/or aspect ratios, and they may be randomly arranged; examples used by the planetary community include the crater roughness model of Veverka and Wasserman (1972), the ''hole'' roughness model of Lumme and Bowell (1981), and Helfenstein's (1988) synthetically cratered landscape. The third category of models are strictly random and consist only of a specified distribution of surface heights or slopes and (often) some statistical relationship between adjacent elements. Connecting three points on such a surface (two on a profile) with straight lines forms a ''facet''; therefore, these models are also referred to as facet models. Examples of this last model type include those used by Hagfors (1964), Beckmann (1965), Smith (1967a), Wagner (1967), and Hapke (1984). Because nature is rarely deterministic when shaping planetary surfaces, the randomized models of the second and third categories are often more applicable to the general scattering problem. Real surfaces are usually (if not always) quantified by measuring surface heights at regular intervals, i.e., by measuring a profile (e.g., Farr 1992, Campbell and Garvin 1993, etc.). For this reason, facet models are often better suited for quantitative or statistical comparisons to real surfaces.

One difficulty with the random models listed above is the lack of an intrinsic or explicit scale dependence. Several (e.g., Beckmann 1965, Smith 1967a, Wagner 1967) explicitly assume that there is no scale dependence in parameters such as the root-mean-square (RMS) height, σ, an assumption commonly referred to as stationarity. However, it is now recognized that real surfaces are not stationary and that the RMS height (among other parameters) is a function of the scale at which it is measured (cf., Sayles and Thomas 1978). Figure 1 illustrates how commonly measured topographic parameters vary with scale on a basalt flow in the Lunar Crater Volcanic Field, Nevada (Arvidson *et al.* 1991, Shepard *et al.* 1995). Other models (e.g., Lumme and Bowell 1981, Hapke 1984) assume that the roughness varies with scale or extends to all scales. While this is more realistic than those models listed above, it is still restrictive in the sense that the scale dependence cannot be varied. Furthermore, the scale dependence is not made explicit, making it difficult to evaluate its applicability to natural surfaces.

The measured behavior of real surfaces (Fig. 1) suggests that a single parameter surface roughness model, such as those above, is insufficient to quantitatively or statistically describe their form. Rather, there must be some knowledge of the distribution of surface heights or slopes *at a single scale* and a function that expresses the change in surface properties with scale. Theoretically, there is no restriction on the form of this function. However, empirical analysis of numerous natural surfaces has revealed a relatively simple functional form which has been termed self-affinity or, more commonly, ''fractal'' (Mandelbrot 1982). Over a range of scales, spanning from micrometers to kilometers, relationships observed to hold for many natural surfaces include

$$\sigma(L) = \sigma(L_0)\left(\frac{L}{L_0}\right)^H \tag{1}$$

$$s(\Delta x) = s(\Delta x_0)\left(\frac{\Delta x}{\Delta x_0}\right)^{H-1}, \tag{2}$$

where $\sigma(L)$ is the RMS height for a profile of some length, L, L_0 is the length of some reference profile (often chosen to be 1 unit in length), $s(\Delta x)$ is the RMS slope of a surface between points a distance Δx apart, Δx_0 is, again, a reference distance of arbitrary length, and H is a parameter variously referred to as the Hurst exponent or Hausdorff measure, $0 < H < 1$ (Hastings and Sugihara 1993, Shepard

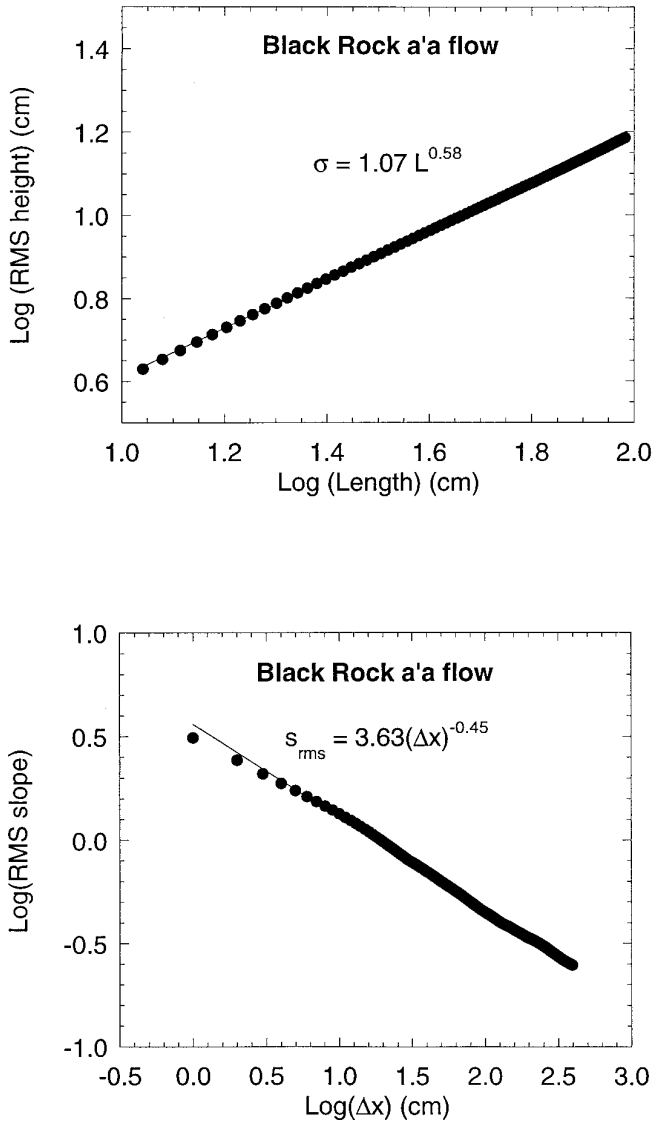

FIG. 1. RMS heights and slopes of the Black Rock lava flow (Lunar Crater Volcanic Field, Nevada) as a function of the measurement scale.

et al. 1995, Turcotte 1997). In Eqs. (1) and (2), $\sigma(L_0)$ and $s(\Delta x_0)$ are "anchoring" parameters and H is the parameter that describes how these values change with scale. To illustrate the role of H, Fig. 2 shows three synthetic fractal profiles which have the same RMS slope at the smallest scale, but different values of H. Note that, consistent with Eq. (1), the surfaces with higher H values retain their roughness even at large scales while those with low H do not. A commonly reported parameter is the fractal dimension, D, which is related to H by

$$D = 2 - H$$
$$D = 3 - H. \quad (3)$$

The first expression in (3) is applicable to a profile, and the second is applicable to a surface (Mark and Aronson 1984, Shepard *et al.* 1995, Turcotte, 1997). To avoid switching back and forth between fractal dimensions for profiles and surfaces, we will primarily utilize the Hurst exponent, H, in this paper.

Like any model, fractals have limitations. The most significant of these is the implicit assumption that the surface is "noise." As a result, fractals cannot easily *forward* model (or generate) surfaces like those of category two above, i.e., a randomized landscape composed of discrete geologic features (e.g., craters, river channels, etc.). Nevertheless, fractals are a robust tool for *reverse* modeling homogeneous regions of random structure. In other words, given specific examples of any homogeneous landscape from category two or three (i.e., surfaces one might encounter in the field), fractals provide a simple, yet powerful way of quantifying their intrinsic scale-dependent surface roughness. A less significant limitation of fractals is the number of required parameters; current roughness models utilize only one (or effectively one as we see below) roughness parameter, while the simplest fractal model incorporates two.

It is not well understood why natural surfaces obey the relationships (or derivatives of them) expressed by Eqs. (1) and (2); the evidence that they do, however, is overwhelming. Figure 1 illustrates this behavior for the basalt flow; both the RMS height and RMS slope obey the scaling relationships of Eqs. (1) and (2) with $H \sim 0.6$. Mark and Aronson (1984) report values of H ranging from 0.1 to 0.96 for a variety of geologic provinces at scales ranging from tens of meters to tens of kilometers. Brown and Scholz (1985) report H values ranging from ~0.4 to 1.0

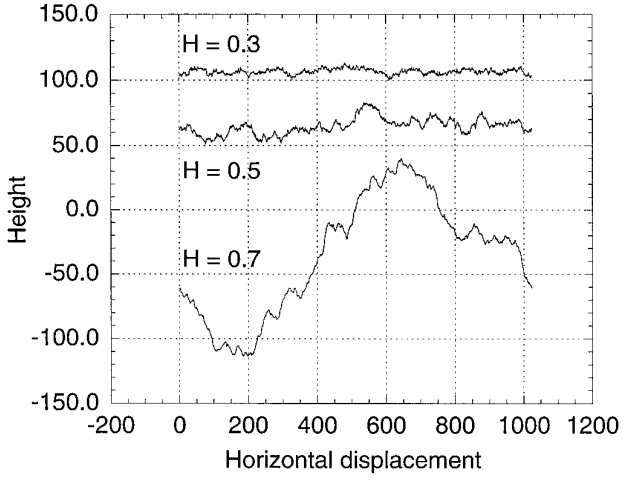

FIG. 2. Plots of three different fractal profiles, offset for clarity, illustrating the effect of different Hurst exponents, H. Each profile has the same RMS slope ($\theta_0 = 45°$) at the smallest horizontal scale, i.e., 1 unit.

for rock surfaces measured at scales of micrometers to centimeters. Our own work with numerous lava flows yielded H values from 0.25 to 0.75 at scales of centimeters to tens of meters (Campbell and Shepard, 1996). Farr (1992) found $H \sim 0.5$ on a wide range of geologic surfaces, also at scales of centimeters to tens of meters. Recent work on the terrestrial planets has shown similar behavior. Haldemann *et al.* (1997, personal commun.) found $H \sim 0.5$ for the terrain around the Mars Pathfinder landing site at scales of centimeters to tens of meters, while Helfenstein *et al.* (1998) report H values 0.5 to 0.7 for undisturbed lunar regolith at scales of micrometers to centimeters.

It has been noted that some surfaces obey different scaling laws over different ranges of scale, i.e., H is itself a function of scale. Mark and Aronson (1984) and Campbell and Shepard (1996) (among others) have speculated that these ''breaks'' in H represent the scales at which different processes dominate the formation and evolution of the surface. As an example, Campbell and Shepard (1996) noted that, on pahoehoe lava flows, centimeter-scale topography obeyed a different scaling law than the meter-scale topography. Field observations revealed the centimeter scales to be dominated by glassy weathering rinds, while meter scales were dominated by constructional flow features.

Rarely reported, but of some importance, is the value of RMS height or slope at an anchoring scale. Campbell and Shepard (1996) found RMS heights on a 1-m-long profile to range from ~8 cm on a very rough a'a flow to ~0.5 cm on a very smooth pahoehoe flow. RMS slopes on the same surfaces measured between points separated by a distance of 1 m ranged from ~13° to ~2°. Shepard *et al.* (1995) reported the RMS slope of a particularly rough a'a basalt flow to be >70° at a scale of 1 cm and ~20° at a scale of 1 m (see Fig. 1). On undisturbed lunar regolith Helfenstein *et al.* (1998) report RMS slopes ranging from 12° to 37° at the millimeter scale.

The above discussion leads us to conclude that fractal surface models are both realistic in their ability to quantify the behavior of natural surfaces, and general enough to quantify a wide range of geologic terrain. Their disadvantages include an assumption that the surface is ''noise'' and a required minimum of two parameters. Their overwhelming advantage is that many real surfaces are observed to obey fractal statistics.

III. COMPARISON OF SHADOWING ON FRACTALS TO OTHER SURFACE TYPES

An inevitable question to address is ''how do surface models that have been used in planetary applications compare with fractal surfaces?'' Straight analytical comparisons are difficult or impossible because of scale issues; parameters such as surface RMS height and autocorrelation length are taken as constants or contain implicit and unspecified scale dependencies in published models, while in fractal models they are functions of scale; i.e., one must agree upon some scale at which these parameters are measured for comparison. We have therefore chosen a more indirect approach and compare the shadowing behavior of these published surface models to the shadowing behavior of fractal surfaces. A benefit of this approach is that we also determine one property of fractal surfaces that can be incorporated into general scattering models, i.e., their shadowing behavior. In making this comparison, we assume that similar shadowing behavior implies similar surface morphology; i.e., the surfaces are statistically similar. It could be argued that any number of different surfaces might be constructed that have similar shadowing behavior. However, our assumption should be reasonable if the surfaces being compared are all strictly random. We therefore restrict ourselves to a comparison with models from category three, i.e., random faceted surfaces, and leave the comparison with models from category two for future analysis.

Methodology

To our knowledge, there is currently no analytic solution to the problem of shadowing on a fractal surface. However, random fractal surfaces are relatively easy to synthesize and ray trace. Therefore, we make our comparisons based upon the shadowing behavior of synthetic random fractal surfaces. We make several assumptions in our numerical simulations which make them compatible with the analytical models to which they will be compared. First, the surface is assumed to be a composite of smooth facets and geometric optics applies, i.e., the facets are large with respect to the wavelength. Second, the facets are distributed uniformly in azimuth. Further, secondary reflections, i.e., multiple scattering, from adjacent facets are ignored. Finally, the distribution of facet slopes about a mean horizontal plane is assumed to be Gaussian. This latter assumption is consistent with observations on many real surfaces, with fractal models (Hastings and Sugihara 1993), and with the analytic surface models we examine.

Shadows created on a fractal surface by a collimated source behave identically to shadows created on the series of profiles that make up that surface, i.e., the three-dimensional shadowing problem can be reduced to a two-dimensional one. Because the creation of fractal surfaces is computationally more expensive than profiles, we chose to work with fractal profiles for the numerical component of this work. We emphasize, however, that the results obtained by examining fractal profiles are identical to those that we would obtain from a fractal surface, and we will therefore interchangeably refer to the shadowing behavior

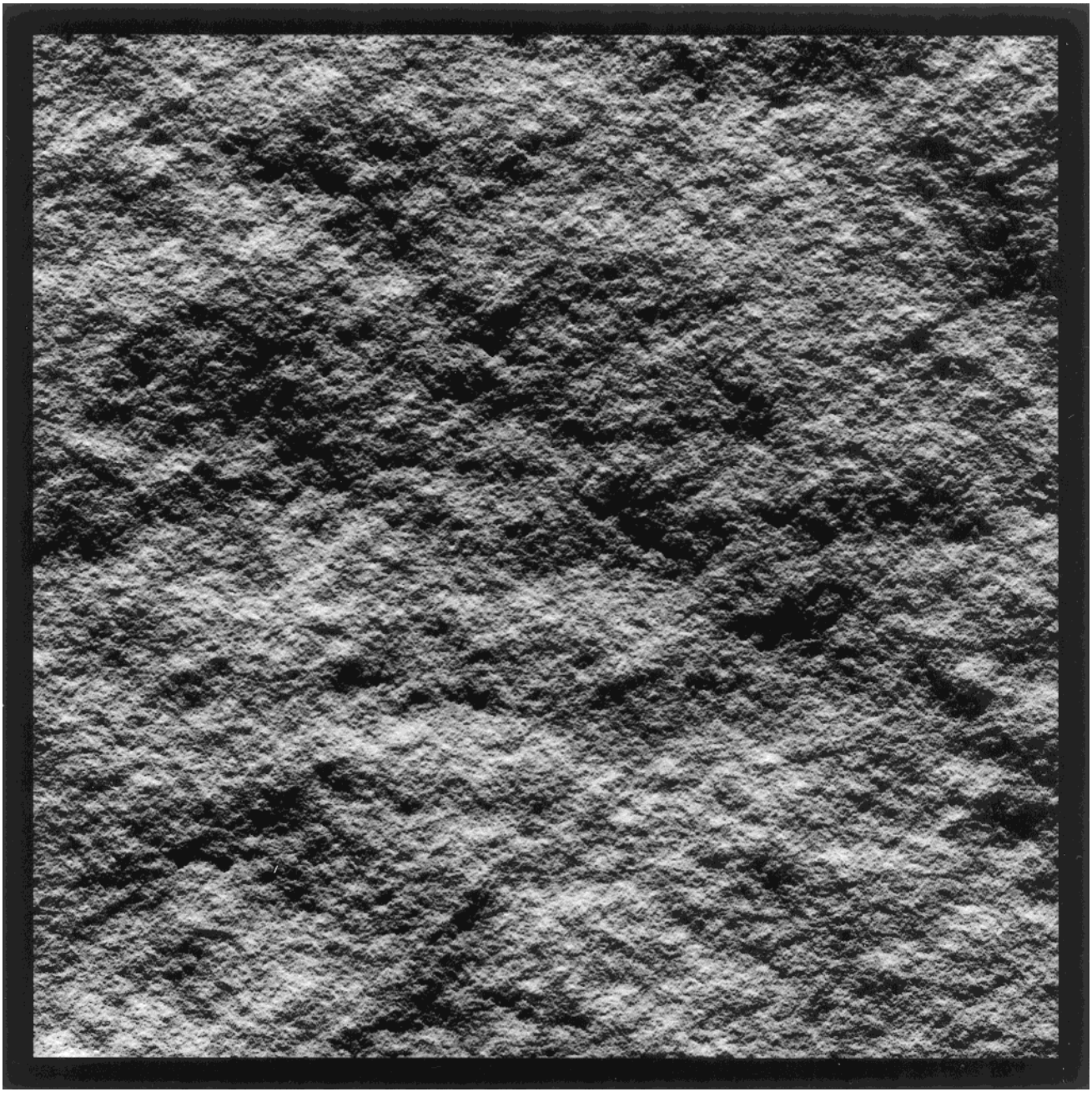

FIG. 3. Rendered image of a synthetic fractal surface, $H = 0.7$, $s_0 = \tan(45°)$, incidence angle = 45°. The rendering assumes the surface facets obey a Lommel–Seeliger scattering law.

of fractal surfaces or fractal profiles. To convey a sense of the realism of textures generated by fractal algorithms, Fig. 3 shows an example of a random fractal surface we generated, shaded using a ray-tracing algorithm, and rendered assuming a Lommel–Seeliger scattering law.

Using the spectral method outlined by Voss (1988) and Turcotte (1997), we generated fractal profiles with Hurst exponents (H) of 0.1, 0.3, 0.5, 0.7, and 0.9 and five different values of $\theta_0 = \tan^{-1}(s_0)$ ranging from 10° to 50°. The values of the Hurst exponent were verified using the variogram method (Shepard *et al*. 1995). The parameter $s_0(=\tan\theta_0)$ is the RMS slope for these surfaces at the smallest horizontal interval. Slopes of the profile at larger scales can be calculated from Eq. (2). It is necessary to specify a lower boundary on the facet size of a fractal profile or surface because, if allowed to decrease in scale indefinitely, the RMS slope

will go to infinity (Eq. (2)). We discuss the interpretation of this in more detail below.

For each of the generated profiles, we assumed parallel illumination at a range of incidence angles (angle from nadir), i, from 10° to 80°. The emission angle was set at 0°, i.e., nadir-viewing, and a ray-tracing algorithm run to determine the fraction of the profile in shadow. Because each fractal profile generated is only a single realization of a random process, each simulation was run under the same conditions 10 times (i.e., 10 different fractal profiles with the same statistical behavior) from which the mean shadowing behavior was determined. All profiles were 100,000 units long. Half of this profile was used only as a border to ensure adequate shadowing behavior for points on the edge of the surface. This relatively large border is required for low values of H (0.1–0.3) to ensure accurate shadowing statistics. Because shadowing is an anisotropic operation, each profile was illuminated from both sides for comparative purposes and to obtain better averaging statistics.

Fractal Shadowing Function Properties

Table I lists the fraction of the profile (or surface) *not* shadowed, S, as a function of i, H, and θ_0, along with the range of shadowing behavior observed for each profile. In general, the higher values of H (lower fractal dimensions) exhibit wider variation in shadowing behavior across the multiple realizations. Figure 2 illustrates why this is the case. Surfaces with higher H values have more extreme values of surface height; i.e., for a given profile length, they tend to be more rugged. This gives rise to greater statistical variations in the amount of surface in shadow. Conversely, surfaces with low H values have height distributions which remain close to the mean value—large scale topography is conspicuously absent.

Figure 4 illustrates the effect of varying H for a constant RMS slope, in this case 30°. Note that surfaces which maintain more of their initial roughness as scale increases, i.e., those with higher H values, are shadowed to a greater degree than those with low H values. Figure 5 illustrates the shadowing function for surfaces with the same value of H, in this case 0.5, but different s_0. Not unexpectedly, for a given value of H, larger RMS slopes at the smallest scales lead to increased shadowing. We have found the following empirical relationship to provide excellent approximations to the shadowing function, S:

$$S(i, \theta_0, H) = 1 - \frac{1}{2}\sum_{n=1}^{\infty} \frac{1}{2.3^{n-1}} \operatorname{erfc}\left(\frac{n^{1-H}}{\sqrt{2}\tan(i)\tan(\theta_0)}\right), \quad (4)$$

where erfc is the error function complement, i is the incidence angle, and θ_0 is the RMS slope at the smallest facet scale, as defined earlier. In practice, the summation needs only to be carried to six terms or less to converge to within 1% of the final value. Equation (4) is found to reproduce the majority of the data in Table 1 to within 0.01, well within the expected uncertainties of our numerical procedure. The reproduction is worse for high H, high θ_0 surfaces, although still within the range of values quoted in the table. Equation (4) also has interesting similarities to the analytic formulations that we examine below.

Comparison to Analytic Models

We chose to compare the numerical results found above to four random surface models for which shadowing functions were derived. In all but one of these models (Hapke 1984), the shadowing function is derived for the case of nadir-viewing only. Hapke's (1984) model is more general in that any combination of incidence, emission, and phase angle is permitted and that it is intimately convolved into a general scattering model. We will examine only the nadir-viewing case here to maintain consistency with the other models. In what follows, we briefly describe the surface model, present a summary of the shadowing function, and compare it with the shadowing behavior found on a fractal surface. We will refer to ''surface model'' and ''shadowing model'' synonymously since we are vicariously equating surface behavior to shadowing behavior.

A. Beckmann shadowing model. Beckmann (1965) derived his shadowing model for the study of microwave quasi-specular scattering. We include this model because the surface description is identical to that assumed by many in the radar scattering community (e.g., Hagfors 1964). We note, however, that the shadowing formula derived in this work has been the subject of some controversy because attempts to verify it using numerical simulations were not successful (Brockelmann and Hagfors 1966).

Beckmann (1965) assumed that the surface in question is stationary and characterized by a Gaussian height distribution and an arbitrary autocorrelation function, $B(x)$. Although it was not included in this derivation, Beckmann (1965) foresaw the necessity of fractal models in his discussion on the relative importance of small and large scale topography. Beckmann's shadowing function is

$$S(i) = \exp\left[-\frac{1}{4}\tan(i)\operatorname{erfc}\left(\frac{\cot(i)}{\sqrt{2|B''(0)|}}\right)\right], \quad (5)$$

where $S(i)$ is the fraction of surface not in shadow, i is the incidence angle (from nadir), erfc is the error function complement, and $B''(0)$ is the second derivative of the surface autocorrelation function analyzed at a lag of 0. Explicit expressions for the argument of the error function complement are

TABLE I
Average Shadowing Function (Fraction of Surface Not in Shadow) for 10 Fractal Surfaces with Hurst Exponent, H, and RMS Slope at the Smallest Scale, s_0[a]

H	ι	$\theta_0 = 10°$	$\theta_0 = 20°$	$\theta_0 = 30°$	$\theta_0 = 40°$	$\theta_0 = 50°$
0.1	10°	1.000 ± 0.000	1.000 ± 0.000	1.000 ± 0.000	1.000 ± 0.000	1.000 ± 0.000
	20°	1.000 ± 0.000	1.000 ± 0.000	1.000 ± 0.000	0.999 ± 0.001	0.989 ± 0.001
	30°	1.000 ± 0.000	1.000 ± 0.000	0.999 ± 0.000	0.980 ± 0.001	0.925 ± 0.001
	40°	1.000 ± 0.000	0.999 ± 0.001	0.980 ± 0.001	0.920 ± 0.001	0.824 ± 0.001
	50°	1.000 ± 0.000	0.989 ± 0.001	0.925 ± 0.001	0.824 ± 0.001	0.709 ± 0.001
	60°	0.999 ± 0.001	0.943 ± 0.001	0.824 ± 0.001	0.701 ± 0.001	0.581 ± 0.002
	70°	0.980 ± 0.001	0.824 ± 0.001	0.671 ± 0.002	0.544 ± 0.001	0.434 ± 0.002
	80°	0.824 ± 0.001	0.581 ± 0.002	0.434 ± 0.002	0.334 ± 0.002	0.256 ± 0.002
0.3	10°	1.000 ± 0.000	1.000 ± 0.000	1.000 ± 0.000	1.000 ± 0.000	1.000 ± 0.000
	20°	1.000 ± 0.000	1.000 ± 0.000	1.000 ± 0.000	0.999 ± 0.001	0.989 ± 0.001
	30°	1.000 ± 0.000	1.000 ± 0.000	0.999 ± 0.001	0.980 ± 0.001	0.923 ± 0.002
	40°	1.000 ± 0.000	0.999 ± 0.001	0.980 ± 0.001	0.918 ± 0.002	0.818 ± 0.002
	50°	1.000 ± 0.000	0.989 ± 0.001	0.923 ± 0.002	0.818 ± 0.002	0.695 ± 0.001
	60°	0.999 ± 0.001	0.942 ± 0.001	0.818 ± 0.002	0.686 ± 0.001	0.558 ± 0.002
	70°	0.980 ± 0.001	0.818 ± 0.002	0.654 ± 0.001	0.520 ± 0.002	0.407 ± 0.002
	80°	0.818 ± 0.002	0.558 ± 0.002	0.407 ± 0.002	0.306 ± 0.002	0.229 ± 0.002
0.5	10°	1.000 ± 0.000	1.000 ± 0.000	1.000 ± 0.000	1.000 ± 0.000	1.000 ± 0.000
	20°	1.000 ± 0.000	1.000 ± 0.000	1.000 ± 0.000	0.999 ± 0.000	0.989 ± 0.000
	30°	1.000 ± 0.000	1.000 ± 0.000	0.999 ± 0.001	0.980 ± 0.001	0.920 ± 0.001
	40°	1.000 ± 0.000	0.999 ± 0.001	0.980 ± 0.001	0.915 ± 0.001	0.808 ± 0.002
	50°	1.000 ± 0.000	0.989 ± 0.001	0.920 ± 0.001	0.808 ± 0.002	0.675 ± 0.002
	60°	0.999 ± 0.001	0.940 ± 0.001	0.808 ± 0.003	0.666 ± 0.002	0.532 ± 0.002
	70°	0.980 ± 0.001	0.808 ± 0.002	0.632 ± 0.002	0.491 ± 0.003	0.376 ± 0.004
	80°	0.808 ± 0.003	0.532 ± 0.002	0.376 ± 0.004	0.276 ± 0.003	0.202 ± 0.004
0.7	10°	1.000 ± 0.000	1.000 ± 0.000	1.000 ± 0.000	1.000 ± 0.000	1.000 ± 0.000
	20°	1.000 ± 0.000	1.000 ± 0.000	1.000 ± 0.000	0.999 ± 0.001	0.988 ± 0.002
	30°	1.000 ± 0.000	1.000 ± 0.000	0.999 ± 0.001	0.978 ± 0.003	0.910 ± 0.011
	40°	1.000 ± 0.000	0.999 ± 0.001	0.978 ± 0.003	0.903 ± 0.011	0.777 ± 0.021
	50°	1.000 ± 0.000	0.988 ± 0.002	0.910 ± 0.011	0.777 ± 0.021	0.626 ± 0.030
	60°	0.999 ± 0.001	0.932 ± 0.007	0.777 ± 0.021	0.616 ± 0.031	0.472 ± 0.039
	70°	0.978 ± 0.003	0.777 ± 0.021	0.579 ± 0.033	0.431 ± 0.041	0.318 ± 0.047
	80°	0.777 ± 0.021	0.472 ± 0.039	0.318 ± 0.047	0.225 ± 0.051	0.161 ± 0.053
0.9	10°	1.000 ± 0.000	1.000 ± 0.000	1.000 ± 0.000	1.000 ± 0.000	1.000 ± 0.000
	20°	1.000 ± 0.000	1.000 ± 0.000	1.000 ± 0.000	0.999 ± 0.001	0.968 ± 0.098
	30°	1.000 ± 0.000	1.000 ± 0.000	0.998 ± 0.001	0.967 ± 0.019	0.818 ± 0.295
	40°	1.000 ± 0.000	0.999 ± 0.001	0.967 ± 0.019	0.858 ± 0.071	0.637 ± 0.332
	50°	1.000 ± 0.000	0.983 ± 0.010	0.867 ± 0.068	0.699 ± 0.134	0.474 ± 0.285
	60°	0.999 ± 0.001	0.899 ± 0.052	0.699 ± 0.134	0.520 ± 0.190	0.341 ± 0.231
	70°	0.967 ± 0.019	0.699 ± 0.134	0.481 ± 0.187	0.337 ± 0.173	0.226 ± 0.151
	80°	0.699 ± 0.134	0.375 ± 0.179	0.239 ± 0.161	0.170 ± 0.136	0.125 ± 0.102

Note. See text for a discussion of how these numbers are generated.

[a] The error bars indicate the range of the data, i.e., the maximum deviation on either side of the mean. Note that the range in observed shadowing behavior increases significantly for high values of H.

$$\frac{1}{2}\cot(i)\frac{T}{\sigma} \tag{6}$$

for Gaussian autocorrelation and

$$\frac{1}{\sqrt{2}}\cot(i)\frac{T}{\sigma} \tag{7}$$

for exponential autocorrelation, where T is the autocorrelation length. The ratio of RMS height to autocorrelation length observed in Eqs. (6) and (7) is often used in radar general scattering models and has been referred to as the "effective" slope (Campbell and Garvin 1993). Note that a change in the autocorrelation function changes the argument of Eq. (5) only by a constant and does not affect the general shape of the shadowing function. In other words, this model is really a function of a single surface parameter—the effective slope.

While examples of the Beckmann function can be found

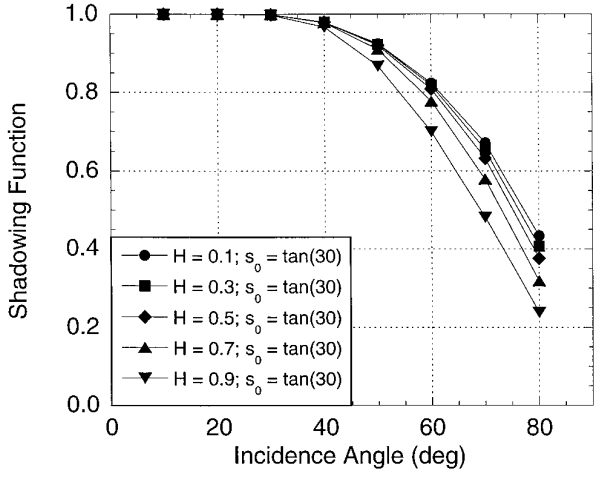

FIG. 4. The shadowing function for ray-traced fractal surfaces with same value of s_0, but different Hurst exponents, H.

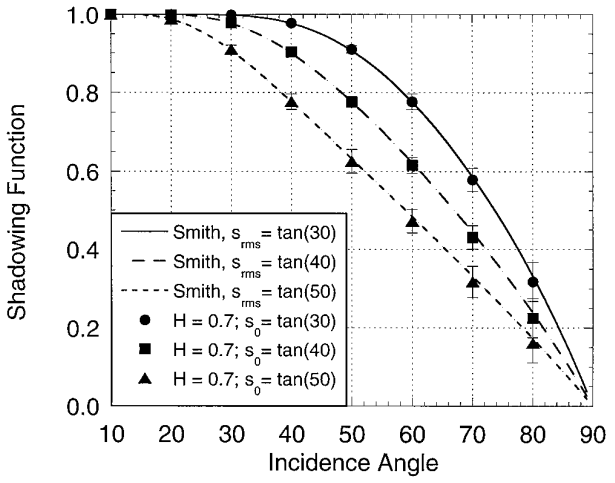

FIG. 6. Comparison of the Smith (1967a) shadowing function and ray-traced fractal profile, $H = 0.7$.

that are reasonably approximated by the shadowing behavior of a fractal surface (for example, the behavior for an effective slope of 47° and a fractal surface, $H = 0.5$, $\theta_0 = 30°$), no systematic relationship appears to exist between the effective slope of the Beckmann function and the fractal θ_0 for any value of H tested. Based on this and the earlier work by Brockelmann and Hagfors (1966), we conclude that either the surface model assumed is an unrealistic one or (more likely) that an error was made in the shadowing derivation.

B. Smith shadowing model. Smith (1967a) derived a shadowing model which he later applied to thermal emission and optical shadowing studies of the Moon (Smith 1967b). Smith's analysis contains similarities to both Beckmann (1965) and Wagner (1967) (below). However, he includes a surface slope distribution (instead of an autocorrelation function) in addition to a height distribution and explicitly assumes that heights and slopes on the surface are uncorrelated. His shadowing solution is

$$S(i) = \frac{\left[1 - \frac{1}{2}\operatorname{erfc}(\cot(i)/\sqrt{2}s_{\mathrm{rms}})\right]}{\frac{1}{2}\left[\left(\frac{2}{\pi}\right)^{1/2}\frac{s}{\cot(i)}e^{-\cot^2(i)/2s_{\mathrm{rms}}^2} - \operatorname{erfc}(\cot(i)/\sqrt{2}s_{\mathrm{rms}})\right] + 1}, \tag{8}$$

where s_{rms} is the RMS surface slope. Note that this is also a single parameter roughness model. We found a close correspondence between Eq. (8) and fractal surfaces with $H = 0.7$ (Fig. 6):

$$s_{\mathrm{rms}} \approx s_0 \qquad \text{for} \qquad H = 0.7. \tag{9}$$

This fit between the Smith model and fractal surface behavior degrades significantly for lower and higher values of H.

C. Wagner shadowing model. Wagner (1967), starting with essentially the same assumptions and using an analytical method similar to Smith (1967a), derives a shadowing function of the form

$$S(i) = \frac{[1 + \operatorname{erf}(v)][1 - e^{-2X}]}{4X} \tag{10}$$

where the roughness term, v, is the same argument found in the Beckmann (1965) expression, (Eqs. (6) and (7)), and X is given by

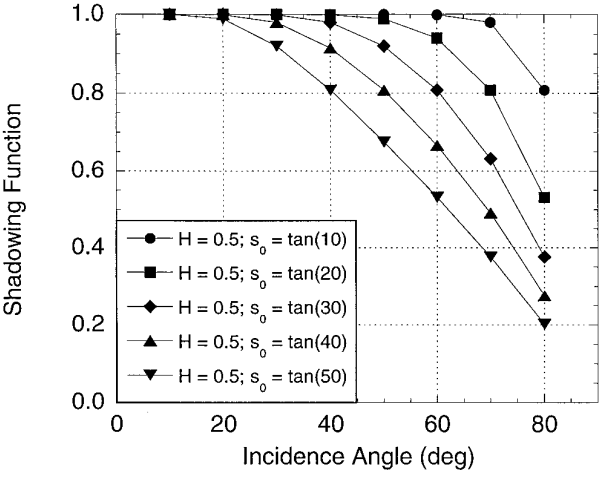

FIG. 5. The shadowing function for ray-traced fractal surfaces with same Hurst exponent, H, but different values of s_0.

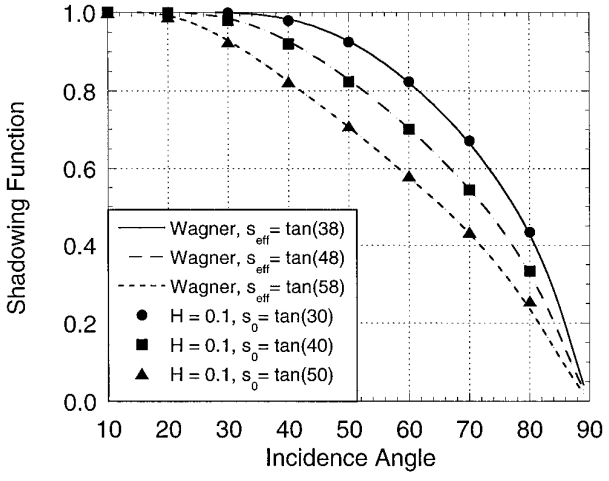

FIG. 7. Comparison of the Wagner (1967) shadowing function and ray-traced fractal profile, $H = 0.1$.

$$X = \frac{e^{-v^2} - \sqrt{\pi} v \operatorname{erfc} v}{4\sqrt{\pi} v}. \tag{11}$$

If we assume that v is given by Eq. (6), i.e., a Gaussian autocorrelation function, then the shadowing observed on a Wagner surface with effective slope, s_{eff}, appears to mimic that of a low H fractal surface if

$$s_{\text{eff}} \approx 1.3 s_0 \qquad \text{for} \qquad H = 0.1. \tag{12}$$

Figure 7 illustrates the shadowing of the Wagner model and fractal surfaces with $H = 0.1$. The ability of the fractal shadowing function to mimic the Wagner model degrades as H increases. As with the Beckmann model, there is no change in the shape of the shadowing curve for different autocorrelation functions.

D. Hapke shadowing model. Because of the popularity and complexity of the Hapke (1981, 1984) model, we discuss its derivation in somewhat more detail than those above. Hapke (1981) derived an approximation to the problem of light scattering and absorption from a regolith or particulate surface. Later, Hapke (1984) improved upon this model by incorporating the effects of rough topography. Unlike the previous models, the Hapke (1984) model incorporates the roughness correction into the "ideal" surface scattering problem, i.e., scattering from a smooth regolith. It can therefore be considered a general scattering model as defined earlier.

In his roughness correction, Hapke (1984) makes the following assumptions: (1) all scattering objects are large with respect to the wavelength, i.e., geometric optics applies; (2) the mean slope of the surface (defined below) is reasonably small, i.e., no overhangs or scarps; (3) multiple scattering between adjacent facets is ignored so that facets in cast shadows contribute no light to the return, even if in the view of the sensor; and (4) the surface slopes obey Gaussian tilt statistics and are isotropically distributed in azimuth. The mean surface slope is defined as

$$\tan \bar{\theta} = \frac{2}{\pi} \int_0^{\pi/2} a(\theta) \tan(\theta)\, d\theta, \tag{13}$$

where $a(\theta)$ is the distribution of surface slopes, and $\bar{\theta}$ is the Hapke roughness parameter. The full Hapke (1984) photometric roughness correction incorporates two effects: (1) the change in the "effective" incidence and emission angles caused by rough topography and illuminating and/or viewing the surface from off-nadir directions and (2) the removal of portions of the surface by cast shadows. Both of these correction factors were derived assuming the same surface model. In this paper, we are not "testing" the full roughness correction as done by Helfenstein (1988). Rather, we are concerned only with the shadowing portion of that correction as a means of comparing Hapke's assumed surface with fractal surfaces.

As noted earlier, the Hapke (1984) shadowing function is significantly more complex than those previously discussed because it accounts for any general configuration of incidence, emission, and azimuth angles. The interested reader is referred to that reference for the full set of equations. However, under the conditions of this work, i.e., observing the surface from directly overhead, the equation can be greatly simplified and is given by

$$S(i) = \cos(i) \left[\cos(i) + \sin(i) \tan(\bar{\theta}) \frac{\exp\left(-\frac{1}{\pi} \cot^2(\bar{\theta}) \cot^2(i) \right)}{2 - \exp\left(-\frac{2}{\pi} \cot(\bar{\theta}) \cot(i) \right)} \right]^{-1}. \tag{14}$$

The shape of the Hapke shadowing function is nearly indistinguishable from the observed shadowing on a fractal surface with $H = 0.5$ and obeying

$$\tan \bar{\theta} \approx 0.7 s_0 \qquad \text{for} \qquad H = 0.5. \tag{15}$$

Figure 8 shows a comparison of the shadowing behavior predicted by Eq. (14) and that observed from the synthetic fractal surfaces obeying Eq. (15). The goodness of fit observed in Fig. 8 degrades significantly for higher and lower values of H. We note that fractal surfaces or profiles with this specific value for H are often referred to as

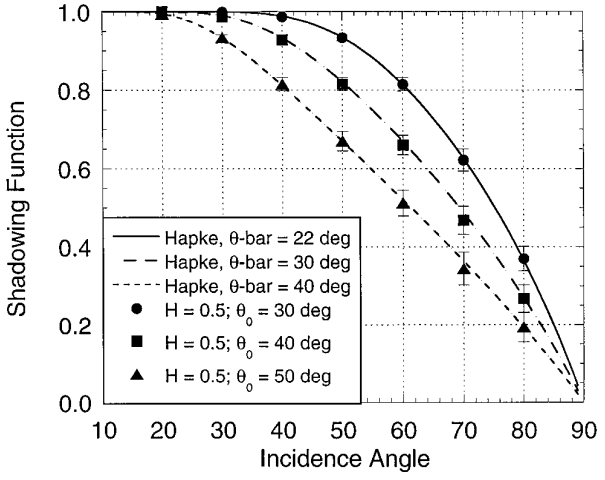

FIG. 8. Comparison of the Hapke (1984) shadowing function and ray-traced fractal profile, $H = 0.5$.

"Brownian" and that Brownian surfaces are fairly common on Earth (Farr 1992, Shepard *et al.* 1995, Campbell and Shepard 1996).

Generality of Fractal Surface Models

To briefly summarize the results of the previous section, we have found that the Smith, Wagner, and Hapke shadowing models can be approximated by the shadowing behavior of a fractal surface with specific values of H and a constant, linear relationship between their respective roughness parameters and the fractal surface parameter s_0. The Beckmann (1965) model could not be reproduced in any systematic fashion. As noted, however, previous numerical work by Brockelman and Hagfors (1966) has cast doubt on the validity of its derivation and we therefore exclude it from further consideration.

In our analysis, we have made the assumption that similar shadowing behavior implies similar surface statistical behavior. If valid, then we can reasonably conclude that each of the above surface models may be approximated by a specific case of a general fractal surface model, i.e., a random surface with a power law scaling dependence obeying Eqs. (1) and (2). While this could suggest that one or more are special cases of a fractal model (with fixed H), we cannot demonstrate this with our current empirical results. Given the range of fractal behavior observed on natural surfaces and the ability of fractal surfaces to mimic the analytic models above, we suggest that incorporating a fractal surface model into general scattering models would make them applicable to a wider range of planetary surfaces than possible utilizing these or any other single parameter models.

IV. THE SCALE OF SURFACE SHADOWING

As we have noted throughout this work, surface roughness changes with scale. Therefore, a question of great practical interest is the scale of surface roughness that is being detected by optical shadowing and photometric models. All of the conclusions and speculations offered below are based only on the observed shadowing behavior of fractal surfaces. However, because shadowing is an important and integral component of any model that purports to extract roughness information remotely, we suggest that our discussion will have relevance to photometric roughness models in general.

Confirmation and Extension of Previous Studies

In the Beckmann (1965), Smith (1967a), and Wagner (1967) models, the scale of surface roughness was never directly addressed. Hapke (1984), however, explicitly assumed that surface roughness, and therefore shadowing, occurred at all scales. He suggested, though, that the surface reflectance would be dominated by the largest surface slopes, and that these would occur at the smallest scales since this is the range at which surface material strength and particle cohesiveness dominate over gravity. Helfenstein (1988) was the first to test these hypotheses using a synthetically cratered and illuminated surface. He found that the photometrically derived value of Hapke's $\overline{\theta}$ was equivalent to the value measured from the topographic model at the smallest faceted scales. He further reasoned that $\overline{\theta}$ was an integrated parameter describing the roughness of all scales below the resolution of the sensor and above the size of the incident wavelength. Helfenstein's results and interpretation were, however, based on a single realization of a randomly cratered surface. We believe that our numerical experiment can extend these results to a much wider range of surfaces, and provide additional insight into the physical interpretation of $\overline{\theta}$ or related parameters.

We first address the issue of the dominant surface scale at which shadowing occurs. Our results suggest that the *smallest faceted scale* is the dominant scale for surface shadowing. This does not mean that the smallest scale is the only one to contribute to shadows on a surface, but only that it contributes a much larger share than any other scale. Take the example of a fractal Brownian surface ($H = 0.5$) with 1-cm facets and an RMS slope of 40° at this scale. If illuminated at an incidence angle of 50°, then approximately 20% of the surface would be in shadow (Table I). If we took the same surface and added an additional "crenulation" to create facets $\frac{1}{2}$ cm in size, the RMS slope at this scale would be 50° (using Eq. (2)). From Table I, approximately 33% of this surface would be in shadow, meaning that the additional crenulation is responsible for 40% of the overall shadowing. The smallest scales become of even greater importance for $H < 0.5$, and of less importance for $H > 0.5$. This result fits with our intuition of natural surfaces and confirms that of Hapke (1984) and

the findings of Helfenstein (1988). What is new in this work is that we can quantify this intuitive knowledge, and extend it to a much greater range of surface types than previously available.

Next, we address Helfenstein's (1988) interpretation of $\bar{\theta}$ as a measure of the integrated surface roughness. This is entirely consistent with the concept of a fractal surface and the previous discussion. In the above example, a full 40% of the total shadowing was due to the smallest facets. The remaining 60% was due to all the facets at larger scales. Therefore, we can consider the shadowing, and presumably any inferred photometric roughness, to be a function of all the scales of roughness "integrated" together. However, we note that the scale which quantitatively "controls" or "represents" the overall shadowing behavior of the surface is the smallest scale as defined above. Once that scale is set and defined, the remaining surface behavior is defined by the Hurst exponent (or fractal dimension). As before, what is new in this work is that we can now quantify this effect and extend it to a greater range of surface types.

Speculations on the Physical Meaning of "Smallest" Facet

In all of the surface/shadow models considered here there is an explicit assumption that the surface is composed of smooth facets large compared with the wavelength of incident light. As noted earlier, however, facets are a modeler's contrivance—essentially, they are an approximation to the surface structure at scales smaller than those defined or measured. Interestingly, real surfaces continue to be fractal, not faceted, even at the micron scale, i.e., well below the geometric optics limit (cf. Brown and Scholz 1985, Helfenstein *et al.* 1998). Under these conditions, we run into a "fractal paradox" in which every surface should be completely, or at least largely, shadowed. Since this is not observed, we wish to know the scale on a real surface at which the roughness "stops" and therefore corresponds to the "faceted" scale extracted from an analysis that includes shadowing behavior.

We must first carefully define what is meant by "roughness." Fractal surfaces obey two basic relationships (Eqs. (1) and (2)). First, the RMS height of a surface decreases as the scale of measurement decreases. Second, RMS slope increases as scale decreases. Although the two may seem incongruous, they are a result of self-affinity, i.e., the vertical scaling is "slower" than horizontal scaling. A surface may be considered "smooth" or faceted once vertical deviations are approximately 1/10th the size of the wavelength, i.e., the Rayleigh criterion for roughness. Several geologic agents could create surfaces which meet this requirement, including eolian abrasion by submicrometer dust, glacial or fault-induced polishing, and compositionally dependent jointing and/or weathering. However, under most geologic conditions, deviations of this small magnitude are not realized until the horizontal scales approach the order of a wavelength, again below the scales at which geometric optics are valid.

Given the discussion above, we hypothesize that the scale of roughness that dominates shadowing, and by extension photometric roughness, is the smallest scale at which shadows are still existent. In other words, we are suggesting that one or more processes remove shadows below some measurable scale, thereby rendering these scales effectively "invisible" to photometry and giving the appearance of a "faceted" surface. In support of this hypothesis is the recent observation of Helfenstein *et al.* (1998) that values of Hapke's $\bar{\theta}$ measured from undisturbed lunar topography at submillimeter scales are systematically larger than those estimated from photometry.

Two physical mechanisms can cause shadows to be effectively removed, both related to initial assumptions in most shadowing models. First, at scales approaching the wavelength of incident light, the diffraction of light around grains becomes a significant effect and shadows no longer exist. Under these conditions, one must assume that the shadowing behavior observed is dominated by the scale at which the assumptions of geometric optics become invalid, i.e., somewhat greater than the wavelength of incident light.

Multiple scattering is a second mechanism which can effectively remove shadows. Higher order scattering events between adjacent particles or facet-like structures may become significant as the surface roughens and/or single scattering albedo increases. Under these conditions, contrast is reduced, and shadows become increasingly bright. Buratti and Veverka (1985) experimentally demonstrated that multiple scattering on a high albedo rough surface reduces shadow contrast and creates the appearance of a smoother surface. We speculate that this effect may be of importance, even on relatively dark surfaces, as the RMS slopes increase dramatically at millimeter or smaller scales. As adjacent areas of the surface increasingly expose more surface area to one another, light from transmission through adjacent particles and/or multiple surface reflections may rival the incident light on surfaces tilted away form the source and brighten the shadows, thereby reducing or removing contrast on an otherwise rough microstructure. In addition to the critical role of the single scattering albedo, other factors contributing to this effect may include the single particle scattering phase function and particle size distribution. The "facet" scale would therefore be dependent upon intrinsic physical properties as well as the topographic expression of the surface. This interpretation suggests a fundamentally different treatment of multiple scattering in shadowing and photometric roughness modeling. Rather than a property that invalidates traditional photometric models, we suggest that multiple scattering

may be a surface property that *defines* the scale to which these models are most sensitive.

The discussions above suggest that the interpretation of surface roughness based on photometric behavior, and the use of a roughness parameter to compare different planetary surfaces, may be more complex than previously assumed. If our hypothesis is accurate, then it is almost certainly true that the scale at which shadows are ''erased'' will differ for different surfaces, and may differ for the same surface at different wavelengths. This hypothesis can be tested both in the laboratory and/or on a planetary scale. One possible test would involve fitting the full Hapke model to observations of a single surface observed in multiple wavelengths. For the test to be convincing, the surface should have significantly different single scattering albedos at different wavelengths, and no Hapke parameters should be constrained by observations in other wavelengths, i.e., the assumption that some parameters are wavelength independent is not used. While many surfaces have been examined in multiple wavelengths and inverted using the Hapke model, it has generally been assumed that roughness is independent of wavelength.

V. SUMMARY

Based upon the behavior of terrestrial surfaces and a limited sampling from the Moon and Mars, the most realistic and mathematically tractable model of planetary surface topography is a self-affine or fractal model. This type of model requires at least two parameters to define a surface: an RMS height or slope at a known, fixed scale, and a second parameter which controls the rate at which this parameter varies with scale. None of the shadowing and photometric models that we are aware of incorporate this type of surface model and instead utilize a single roughness parameter—typically the RMS slope at some unspecified scale.

We have numerically determined the behavior of shadowing on a wide range of fractal surfaces viewed at nadir and presented an empirical function that reproduces this behavior within the uncertainties of our analysis. A comparison of the shadowing behavior of synthetic fractal surfaces with the Smith (1967a), Wagner (1967), and Hapke (1984) shadowing functions suggests that the surfaces assumed by these authors can be approximated by specific cases of a general fractal surface model.

We have quantitatively demonstrated that the scale which appears to be of greatest importance to shadowing (and, we suggest, to photometric roughness) on a fractal surface is the smallest facet scale. Observations of real surfaces indicate that they are rarely faceted, but rather fractal at practically all measurable scales. Therefore, we hypothesize that the roughness inferred from remote sensing is dominated by the scale at which shadows are effectively removed and that this scale is a function of intrinsic surface roughness and other surface parameters such as single scattering albedo and particle phase function. If this hypothesis is correct, a surface roughness extracted photometrically will have a different physical meaning for different surfaces and for the same surface at wavelengths in which these other parameters differ significantly. While this interpretation precludes the direct comparison of topography from surface to surface, it may provide new insights into the processes that operate on planetary surfaces at the microscale. Future work should include testing this hypothesis and deriving a full photometric correction for fractal surface models.

ACKNOWLEDGMENTS

The authors are grateful to P. Helfenstein for detailed comments that greatly improved this manuscript. We especially thank past (J. Burns) and present (P. Nicholson) editors, and an anonymous associate editor for seeing this manuscript through a contentious review process. This work was supported by NAG5-4000 (M.K.S.) and NAG5-4545 (B.A.C.).

REFERENCES

Arvidson, R. E., M. A. Dale-Bannister, E. A. Guinness, S. H. Slavney, and T. C. Stein 1991. Archive of geologic remote sensing field experiment data, Release 1.0, NASA Planetary Data System. Jet Propulsion Laboratory, Pasadena, CA.

Beckmann, P. 1965. Shadowing of random rough surfaces. *IEEE Trans. Antennas Propag.* **AP-13,** 384–388.

Beckmann, P., and A. Spizzichino 1963. *The Scattering of Electromagnetic Waves from Rough Surfaces*. Pergamon Press, New York.

Brockelman, R. A., and T. Hagfors 1966. Note on the effect of shadowing on the backscattering of waves from a random rough surface. *IEEE Trans. Ant. Prop.* **AP-14,** 621–629.

Brown, S. R., and C. H. Scholz 1985. Broad bandwidth study of the topography of natural rock surfaces. *J. Geophys. Res.* **90,** 12,575–12,582.

Buratti, B. J., and J. Veverka 1985. Photometry of rough planetary surfaces: The role of multiple scattering. *Icarus* **64,** 320–328.

Campbell, B. A., and J. B. Garvin 1993. Lava flow topographic measurements for radar data interpretation. *Geophys. Res. Lett.* **20,** 831–834.

Campbell, B. A., and M. K. Shepard 1996. Lava flow surface roughness and depolarized radar scattering. *J. Geophys. Res.* **101,** 18,941–18,951.

Farr, T. 1992. Microtopographic evolution of lava flows at Cima Volcanic Field, Mojave Desert, California. *J. Geophys. Res.* **97,** 15,171–15,179.

Hagfors, T. 1964. Backscattering from an undulating surface with applications to radar returns from the Moon. *J. Geophys. Res.* **69,** 3779–3784.

Haldemann, A. F. C., R. F. Jurgens, M. A. Slade, and M. P. Golombek 1997. Mars Pathfinder landing site radar properties, *Eos Trans. AGU* **78**(46), Fall Meet. Suppl. F404. [Abstract]

Hapke, B. 1981. Bidirectional reflectance spectroscopy, 1: Theory, *J. Geophys. Res.* **86,** 3039–3054.

Hapke, B. 1984. Bidirectional reflectance spectroscopy, 3: Correction for macroscopic roughness. *Icarus* **59,** 41–59.

Hapke, B. 1986. Bidirectional reflectance spectroscopy. 4. The extinction coefficient and the opposition effect. *Icarus* **67,** 264–280.

Hapke, B., and H. van Horn 1963. Photometric studies of complex surfaces, with applications to the Moon. *J. Geophys. Res.* **68,** 4545–4570.

Hastings, H. M., and G. Sugihara 1993. *Fractals: A User's Guide for the Natural Sciences.* Oxford Univ. Press, Oxford.

Helfenstein, P. 1988. The geological interpretation of photometric surface roughness. *Icarus* **73,** 462–481.

Helfenstein, P., J. Veverka, and M. K. Shepard 1998. Submillimeter-scale topography of undisturbed lunar soils. *Lunar Planet. Sci. Conf. 29th* [abstract], 1648–1649.

Lumme, K., and E. Bowell 1981. Radiative transfer in the surfaces of atmosphereless bodies: I. Theory. *Astron. J.* **86,** 1694–1704.

Mandelbrot, B. B. 1982. *The Fractal Geometry of Nature*. Freeman, New York.

Mark, D. M., and P. B. Aronson 1984. Scale-dependent fractal dimensions of topographic surfaces: An empirical investigation with applications in geomorphology and computer mapping. *Math. Geol.* **16,** 671–683.

Miller, L. S., and C. L. Parsons 1990. Rough surface scattering results based on bandpass autocorrelation forms. *IEEE Trans. Geosci. Remote Sens.* **28,** 1017–1021.

Power, W. L., and T. E. Tullis 1991. Euclidean and fractal models for the description of rock surface roughness. *J. Geophys. Res.* **96,** 415–424.

Sayles, R. S., and T. R. Thomas 1978. Surface topography as a non-stationary random process. *Nature* **271,** 431–434.

Shepard, M. K., R. A. Brackett, and R. E. Arvidson 1995. Self-affine (fractal) topography: Surface parameterization and radar scattering. *J. Geophys. Res.* **100,** 11,709–11,718.

Smith, B. G. 1967a. Geometrical shadowing of a random rough surface. *IEEE Trans. Antennas Propag.* **AP-15,** 668–671.

Smith, B. G. 1967b. Lunar surface roughness: Shadowing and thermal emission. *J. Geophys. Res.* **72,** 4059–4067.

Turcotte, D. L. 1997. *Fractals and Chaos in Geology and Geophysics*. Cambridge Univ. Press, New York.

Veverka, J., and L. Wasserman 1972. Effects of surface roughness on the photometric properties of Mars. *Icarus* **16,** 281–290.

Voss, R. F. 1988. Fractals in nature: From characterization to simulation. In *The Science of Fractal Images* (H. O. Peitgen and D. Saupe, Eds.), pp. 21–69. Springer-Verlag, New York.

Wagner, R. J. 1967. Shadowing of randomly rough surfaces. *J. Acoust. Soc. Am.* **41,** 138–147.